The Structure of Filled and Unfilled Thermotropic Liquid Crystalline Polymer Injection Moldings

C. J. G. PLUMMER,[1,*] B. ZÜLLE,[2] A. DEMARMELS,[2] and H.-H. KAUSCH[1]

[1]Laboratoire de Polymères, Ecole Polytechnique Fédérale de Lausanne, CH-1015 Lausanne, Switzerland;
[2]Asea Brown Boveri, Corporate Research CRBV, CH-5405 Baden-Dättwil, Switzerland

SYNOPSIS

Studies of the microstructure and orientation in thermotropic liquid crystalline polymer injection moldings have been carried out using a variety of techniques to reveal the complex hierarchical structure. The effect of particle filler on the level of molecular orientation in the flow direction appears relatively weak, but at high filler contents, there is a marked disruption of coarse structure in the matrix. © 1993 John Wiley & Sons, Inc.

1. INTRODUCTION

Injection molding of rigid or semirigid chain thermotropic liquid crystalline polymers (TLCPs) is well known to lead to highly complex hierarchical layered structures, with a correspondingly highly inhomogeneous distribution of molecular orientation.[1-16] Molecular orientation in the melt-fill direction is generally found to be highest within a "skin" layer, whereas the orientation of the inner regions is much diminished or even transverse to the flow direction in certain cases. Such orientation distributions are familiar from observations of fiber orientation in injection-molded composites of flexible-chain polymer/short-fiber composites,[17,18] which may be considered as analogous systems to that of a rigid-chain polymer melt, and hierarchical structures may also be seen in the spherulitic morphology of moldings of conventional flexible-chain semicrystalline polymers, e.g., polyacetals.[19,20]

In all cases, the morphological and orientation distributions are found to be strongly dependent on the processing conditions and, in particular, on the melt and mold temperatures and the injection speed. Although detailed analysis of the influence of such factors on the flow behavior of orientable melts during molding is difficult, it has been suggested by Garg and Kenig[1] and Kenig,[21] that mold filling may be characterized in terms of four main processes:

(i) diverging flow close to the inlet gates;
(ii) converging flow at the exit gates;
(iii) fountain flow at the free surface of the advancing melt front; and
(iv) shear flow behind the melt front.

Diverging flow promotes orientation perpendicular to the main melt-fill direction, whereas converging flow has the opposite effect (Fig. 1). Diverging and converging flow are also likely to be important where there is a change in mold cross section as, e.g., in the shoulder regions of a dumbbell-shaped tensile test bar.[1] Thus, if the inlet gate is situated at one of the sample ends, transverse orientation developed at the gate may be compensated as the melt is subsequently squeezed through the constriction in the shoulder region, to an extent that will depend on the precise sample geometry.

In general, during mold filling, there is a gradient in flow velocity, v_i, across the mold width. Assuming that the advancing melt front moves with a velocity $\langle v_i \rangle$, elements of the melt entering the melt cavity at later times, and moving at $v_i > \langle v_i \rangle$, catch up with the melt front and thus experience fountain flow, as illustrated in Figure 1(c). During fountain flow, the melt is in extensional flow, which is known to result in high degrees of molecular orientation in TLCPs, even at low flow rates.[22,23] This orientation is then frozen to form the skin layer as the polymer comes into contact with the cool mold walls.

The regions of the melt that do not reach the flow front are in shear (Poiseuille) flow during mold fill-

* To whom correspondence should be addressed.

Journal of Applied Polymer Science, Vol. 48, 751–766 (1993)
 CCC 0021-8995/93/050751-16

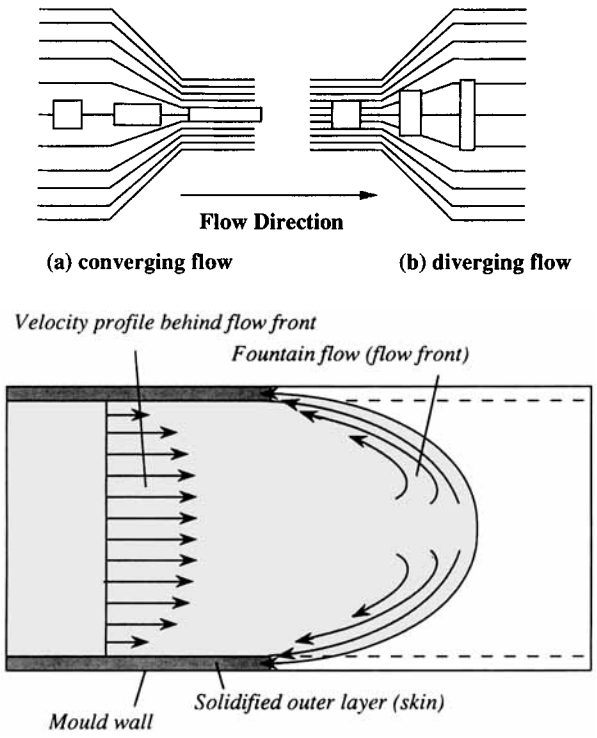

Figure 1 Flow patterns in injection molding of TLCPs.

ing. At the shear rates generally encountered in injection molding, the micron-sized regions of localized orientational correlation observed in quiescent TLCP melts, called "domains," are thought to remain stable and "tumble" rather than elongate in the flow direction, leading to relatively weak orientation.[24-27] Further, owing to the characteristic yielding behavior of TLCP melts, the velocity profile becomes very flat toward the center of the mold, a phenomenon known as *plug flow*. Thus, the central "core" region of the molding may be characterized either by a lack of orientation, or, as is more likely, given the low relaxation rates of TLCP melts, by orientation acquired earlier in its flow history (at the gate, e.g., as discussed above).

Considerable effort has gone into detailed simulation of these processes using mathematical and computational modeling,[28] mostly aimed at short-fiber-filled thermoplastics, but also potentially applicable to the problem of orientation development in TLCPs. However, theoretical models for LCPs are not as yet able to provide working constitutive equations for detailed melt-flow simulation. Hence, current simulations based on finite element analysis (FEA), although of great value to the technologist,[3] are at best only able to give a general indication of the spatial distribution of orientation direction for complex geometries. Moreover, in practice, the structure of even the simplest TLCP moldings, as revealed by TEM of ultrasonically disintegrated fibers[29] and microtomed sections,[30] polarized light microscopy of thin sections, SEM of acid- and plasma-etched surfaces, and fractography, may display many complex levels of hierarchy, extending far beyond that of the basic skin–core structure.[1-15]

Here, we present our own structural observations for a number of different injection moldings. In the case of a series of 3×6 mm^2 cross-section tensile test bars, these have been related to measurements of property variations and molecular orientation, with emphasis on the effect of filler addition.

2. EXPERIMENTAL

The following grades from the Vectra™ (Hoechst-Celanese) "A" series of filled and unfilled TLCPs were investigated: Vectra A950 (unfilled resin); Vectra A515 (15 wt % wollastonite-filled); Vectra A540 (40 wt % wollastonite-filled); and Vectra A130 (30 wt % short glass fiber-filled). Cross-section tensile test bars, 3×6 mm^2, were molded with a mold temperature of 90°C and a mean barrel temperature of 280°C and at a fill-rate of approximately 1 cm^3 s^{-1}. Cross-section dumbbell-shaped tensile test bars, 4×10 mm^2, were injection-molded at a volume fill rate of approximately 10 cm^3 s^{-1} and with mean melt and mold temperatures of 280 and 80°C, respectively. Also investigated were injection-molded plaque samples of Vectra, supplied by Atochem, and 2×10 mm^2 bars of the amorphous TLCP, Ultrax™ KR 4002 (BASF), molded under various injection conditions and supplied by Professor W. Kaiser of HTL Brugg, Switzerland.

Microstructural observations made use of SEM of polished surfaces etched for approximately 10 min in concentrated sulfuric acid, as well as room temperature and liquid nitrogen fracture surfaces. Thin sections were prepared for optical microscopy by hand polishing, the final polish being carried out using 1 μm diamond paste.

For characterization of property distributions within the samples, three basic methods were available, in addition to direct morphological examination:

(i) removal of successive layers from a molding, measuring the modulus each time, from which a modulus–distance profile may be calculated;[1]

(ii) measurement of the properties of the extracted layers themselves;[31] and

(iii) measurement of the orientation distributions within the moldings by wide-angle X-ray scattering (WAXS) or infrared spectroscopy.[12,16]

3. RESULTS

All the TLCP moldings displayed a coarse multilayered structure, sketched in Figure 2. The details of this structure depend to a great extent on geometry, molding conditions, and filler content, but it is broadly representative of the range of TLCP samples types described in the literature.[1-15]

Figure 3 shows the layered structure in reflected light and in transmitted polarized light of a longitudinal section of a 2×10 mm^2 cross-section bar of amorphous Ultrax (melt temperature of 302°C, mean mold temperature of approximately 77.5°C, melt front velocity of 230 mm s^{-1}). This serves to illustrate the correlation between the color bands in reflected light and changes in birefringence and/or scattering in transmitted light, it being possible, e.g., to determine the thickness of the highly oriented skin regions using either method. Reflected light microscopy has been the preferred technique for the systematic characterization of variations in layer distributions in these Ultrax samples[32] and also, for reasons of practical convenience, in our own investigations of the effect of molding conditions on structure development in Vectra.[33,34] Nevertheless, the use of thin layers allows greater resolution (the color contrast in reflected light is hard to see at high magnification) and identification of fine structure and provides information on the local orientation direction.

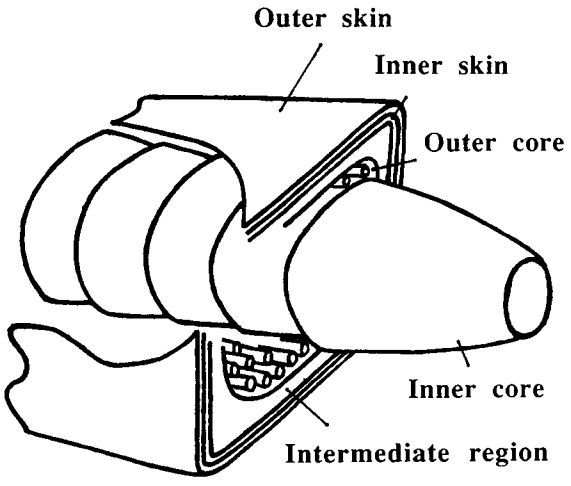

Figure 2 Structure of an injection molding of unfilled TLCP.

Use of thin sections has confirmed that there is a systematic decrease in skin thickness on moving away from the gate in these moldings as reported in Ref. 32. This appears to reflect a "piling-up" of highly oriented material at the melt walls with time during flow, such that the skin thickness in the parts of the mold filled first, i.e., near the gate, reflects the greater time available for the skin to grow.[32] Also noteworthy is the highly chaotic core structure far from the gate in these moldings, which contrasts with the relatively coherent structure observed close to the gate, as shown in Figure 3.

3.1. Detailed Structure of Unfilled Vectra Moldings

As indicated in Figure 2, we have chosen to describe the basic skin–core structure of our moldings in terms of five main subregions. In this section, each region is illustrated in turn, using for the most part micrographs taken from the 4×10 mm^2 cross-section Vectra moldings. These micrographs and the dimensions given below are also characteristic of the 3×6 mm^2 cross-section Vectra moldings. Reference is made to other samples where these show distinct features:

(i) The "outer skin" layer, which extends 40–50 μm into the sample surface and is highly birefringent, indicating high orientation. Polished sections transverse to the flow direction and etched in concentrated sulfuric acid show a characteristic layered structure, as in Figure 4(a). The inner surfaces of outer skin layers separated from the rest of the sample are relatively smooth, as shown in Figure 5(a).

(ii) The "inner skin" layer, approximately 200 μm in total thickness and, like the outer skin, distinguishable from the sample interior by its high birefringence. In contrast with the outer skin, however, etching of polished transverse sections reveals little texture under SEM. Optical microscopy of thin sections, however, reveals a striking banded texture [Fig. 6(a)], and longitudinal freeze fracture surfaces [Fig. 5(b)] are suggestive of a coherent periodic variation in the molecular trajectory along the flow direction. This periodicity, and the associated banding, appear to characterize transient relaxation of a wide range of LCPs subject

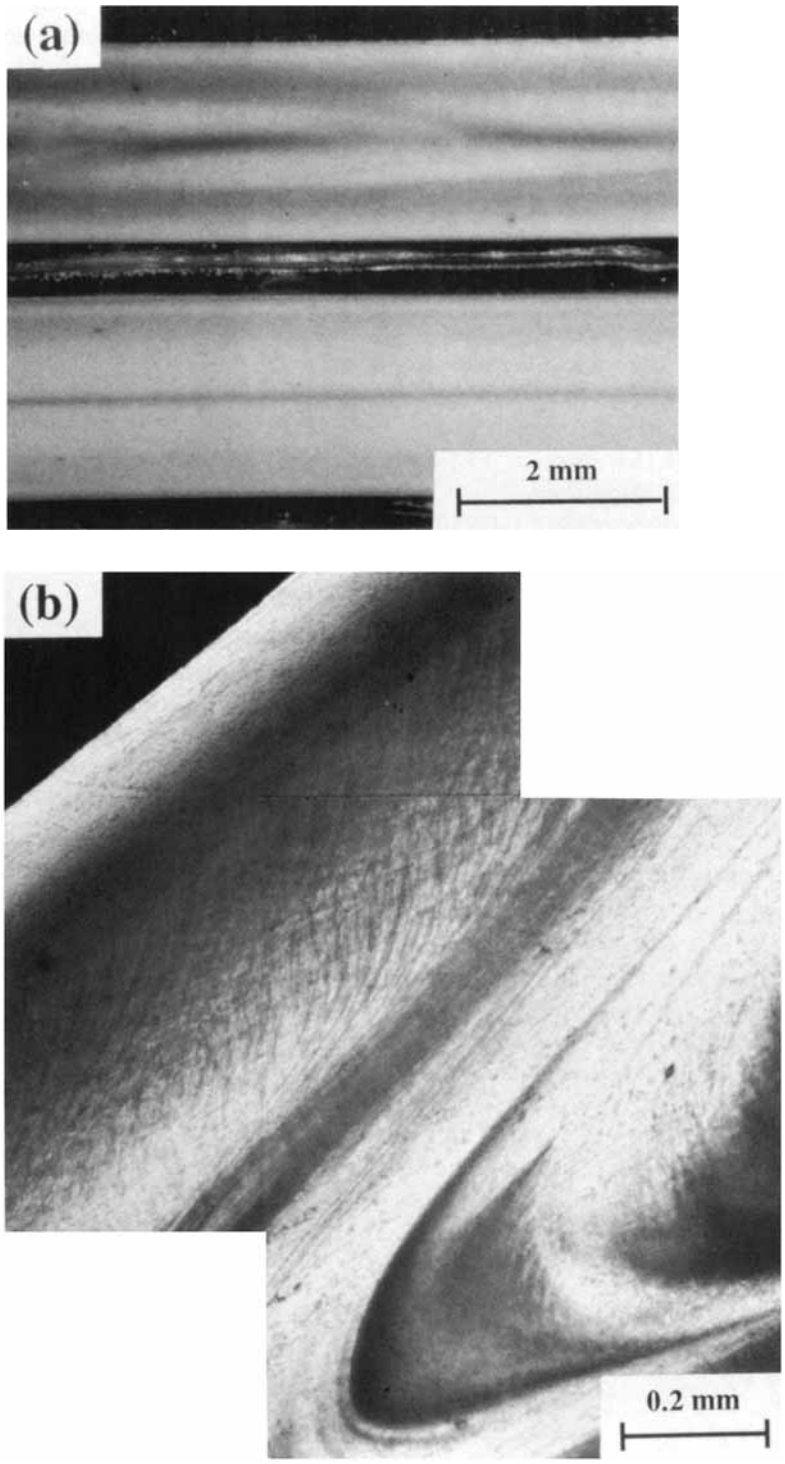

Figure 3 (a) Reflected light micrograph of a longitudinal section of an Ultrax injection molding (above, close to the sample end furthest from the gate; below, close to the gate); (b) transmitted light micrograph under crossed-polarizers of a thin section taken from the end of the sample furthest from the gate.

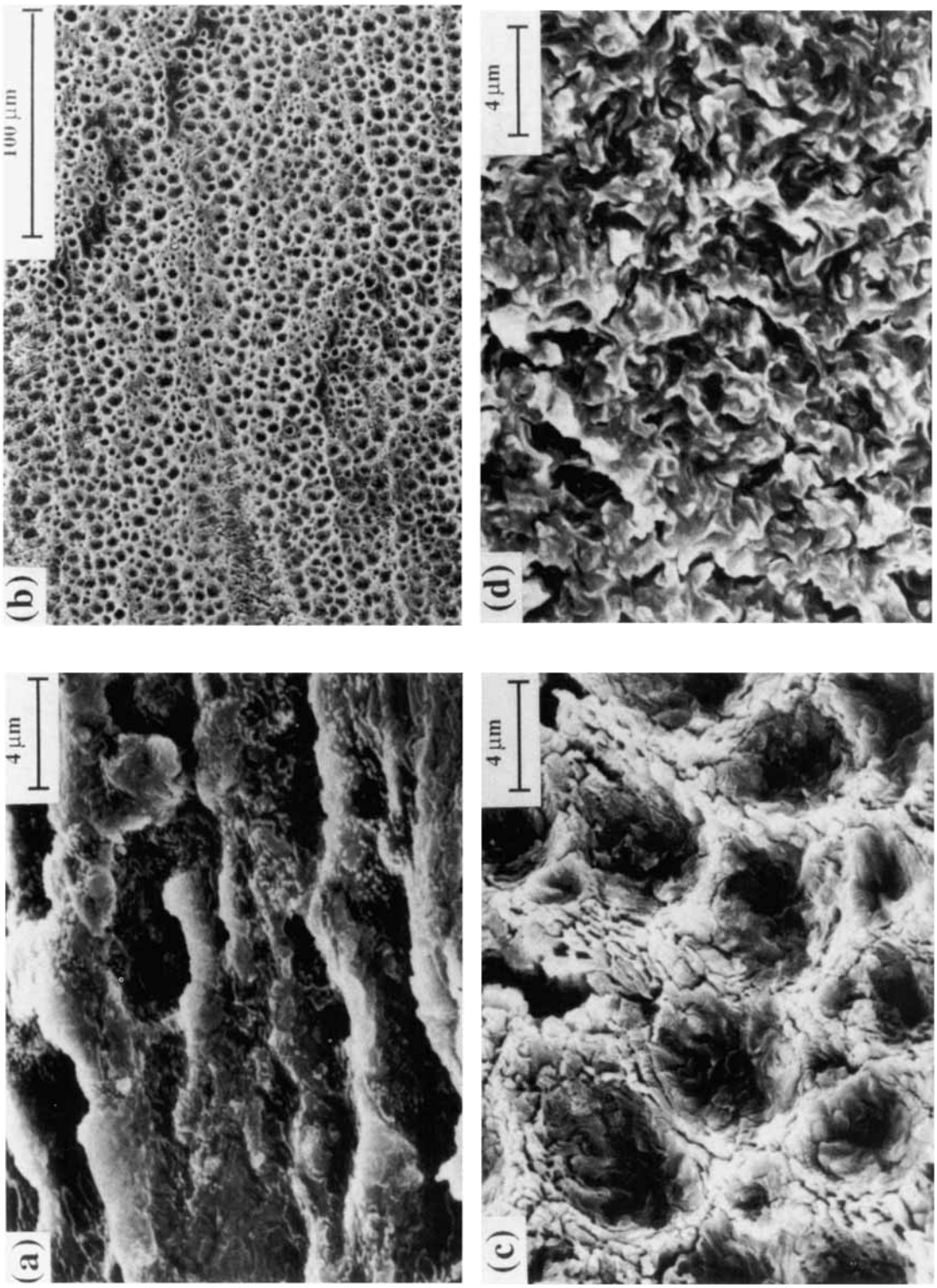

Figure 4 SEM of etched (10 min in concentrated sulfuric acid) transverse sections of unfilled HBA–HNA moldings (A950): (a) outer skin; (b, c) outer core; (d) inner core.

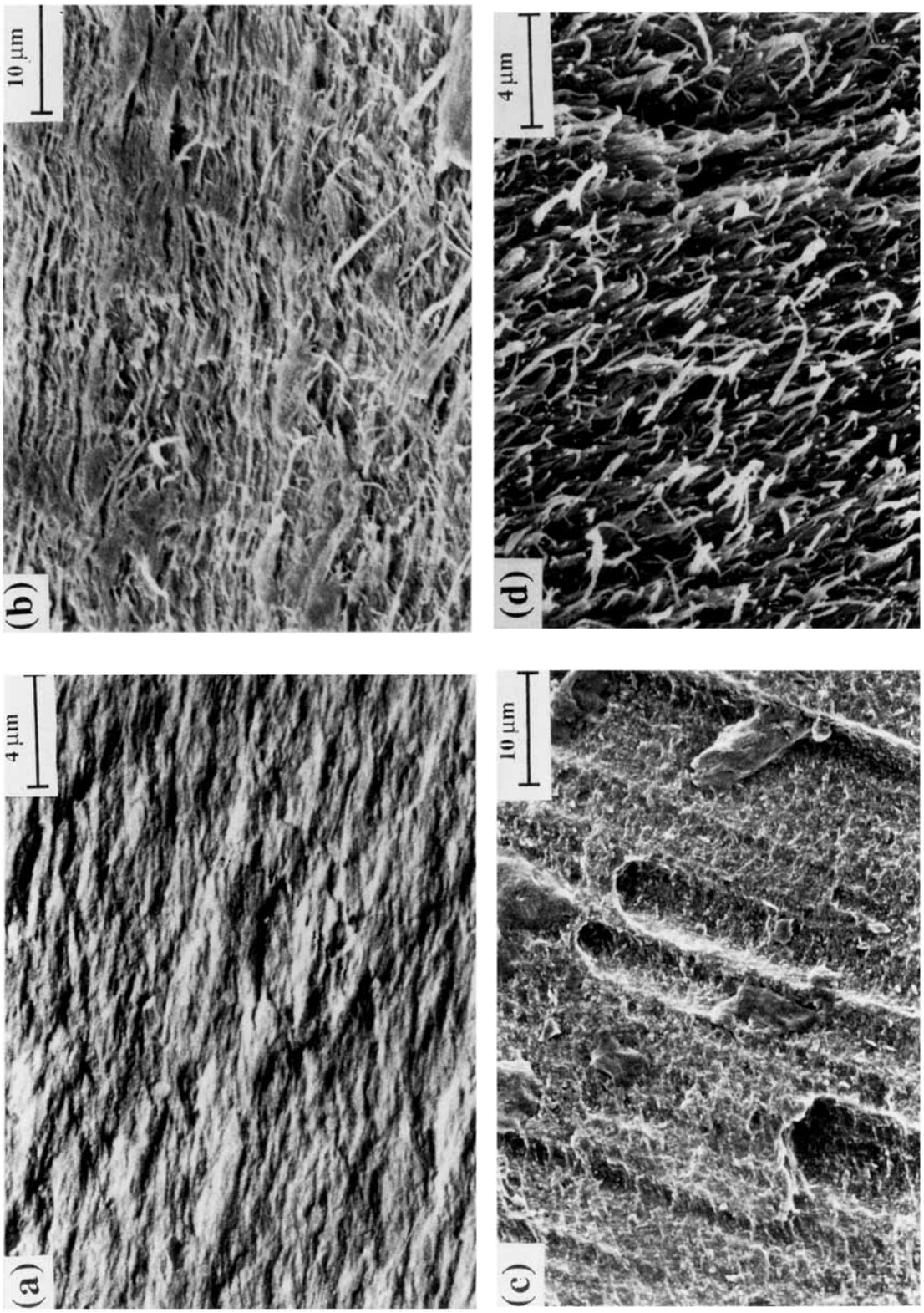

Figure 5 SEM of longitudinal freeze-fracture surfaces of unfilled HBA–HNA moldings (A950): (a) interface between outer and inner skin; (b) interface between inner skin and intermediate region; (c) outer core; (d) inner core (transverse fracture).

to high degrees of shear-induced orientation.[35-40] However, the precise origin of the driving force for such relaxation remains at present unclear.

(iii) The "intermediate" layer, weakly birefringent compared with the skin layers, showing a predominantly tight optical texture [Fig. 6(b)] and, as with the inner skin, no coarse structure under SEM.

(iv) The "outer core," for which SEM of etched transverse sections and longitudinal freeze fracture surfaces reveals a striking fibrillar structure [Figs. 4(b) and (c) and 5(c)]. The fibrils have an approximately circular cross section, with a diameter of approximately 5 microns (consistent with the observations of Tharpar and Bevis[4] and Sawyer and Jaffe[5]), each fibril appearing to consist of an oriented outer cylindrical region and an inner region characterized by structures more akin to the unoriented tight texture. However, some continuity of structure in the inner part of these fibrils may be inferred from their tendency to break up into elongated subfibrils with a diameter of approximately 1 μm (Sawyer and Jaffe[5] identified further levels of fibrillar hierarchy in TLCP moldings and extrudates down to 50 nm).

Considerable variation in the form of the structure in this region is encountered, depending on the mold geometry. In particular, where the mold has a relatively low wall thickness, and high aspect ratio as is the case of the Ultrax moldings, the fibrils appear tapelike, rather than circular.

(v) The "inner core." The bulk structure of the central part of the inner core generally shows features consistent with the tight texture, both optically and under SEM [Fig. 4(d)]. However, superimposed onto the core structure at irregular intervals are approximately conic "flow surfaces" concentric with the core center and which point along the sample axis. During fracture, cracks often run along these flow surfaces, giving locally smooth fracture surfaces as with delamination between the outer and inner skin. Toward the center of the inner core, however, the flow surfaces appear attenuated, the fracture surfaces being predominantly fibrillar [Fig. 5(d)]. Particularly dense and coherent parabolic structures have been observed in the inner core of edge-gated injection-molded plaque samples, being clearly visible as parabolic lines in etched longitudinal sections and optical sections [Fig. 6(c) and (d)].

Figure 7(a)-(c) shows details from the core of an Ultrax thin section, taken from the same sample as in Figure 3, and illustrating the highly coherent parabolic structures in the core. The flow lines are seen to be superimposed onto a tight structure, but toward the outer regions of the inner core and the beginnings of the outer core, there is a suggestion of a banded structure running perpendicular to the flow lines. SEM of fracture surfaces in this region suggests the flow lines in this case to be associated with fibrillar structures [Fig. 7(c)].

3.2. Filled Moldings

In the mineral (wollastonite)-filled Vectra grades, the filler particles themselves have low aspect ratios, with maximum values not exceeding 10. Some random orientation exists in the central core, but in the bulk of the sample barrel, the particles are aligned in the melt-fill direction.

The outermost skin layer, although still essentially layered in structure, is much less coherent than for the unfilled moldings, with many cavities and local distortions of the layered structure, particularly in association with filler particles, and a certain degree of continuity with the inner skin layer. Again, the inner skin layer is distinguished from the intermediate region by its high birefringence and shows localized regions of banding perpendicular to the plane of the layers.

The structure in the outer core often contrasts markedly with that of unfilled moldings; with increasing filler content, the fibrillar structure of the unfilled moldings is progressively broken up, as shown in Figure 8(a)-(c). Thus, the bulk structure of 40 wt % wollastonite-filled HBA–HNA consists mainly of discontinuous layers tangential to the core center [Fig. 8(c)]. Indeed, there is no clear boundary between the different regions in the etched transverse sections, and the main distinction between the inner core and the outer regions is the lack of orientation of filler particles in the core. The conic flow lines observed in the core of unfilled samples are either absent or weakly defined.

As with the mineral-filled moldings, little coarse matrix structure can be seen in the short glass fiber-filled injection moldings. The fibers themselves are highly oriented in the flow direction in the intermediate and outer regions, although considerable disruption of the surface structures occurs owing to "swirling" of the fibers [Fig. 8(d)]. The core of dumbbell-shaped samples generally shows random fiber orientation. In edge-gated plaques, however,

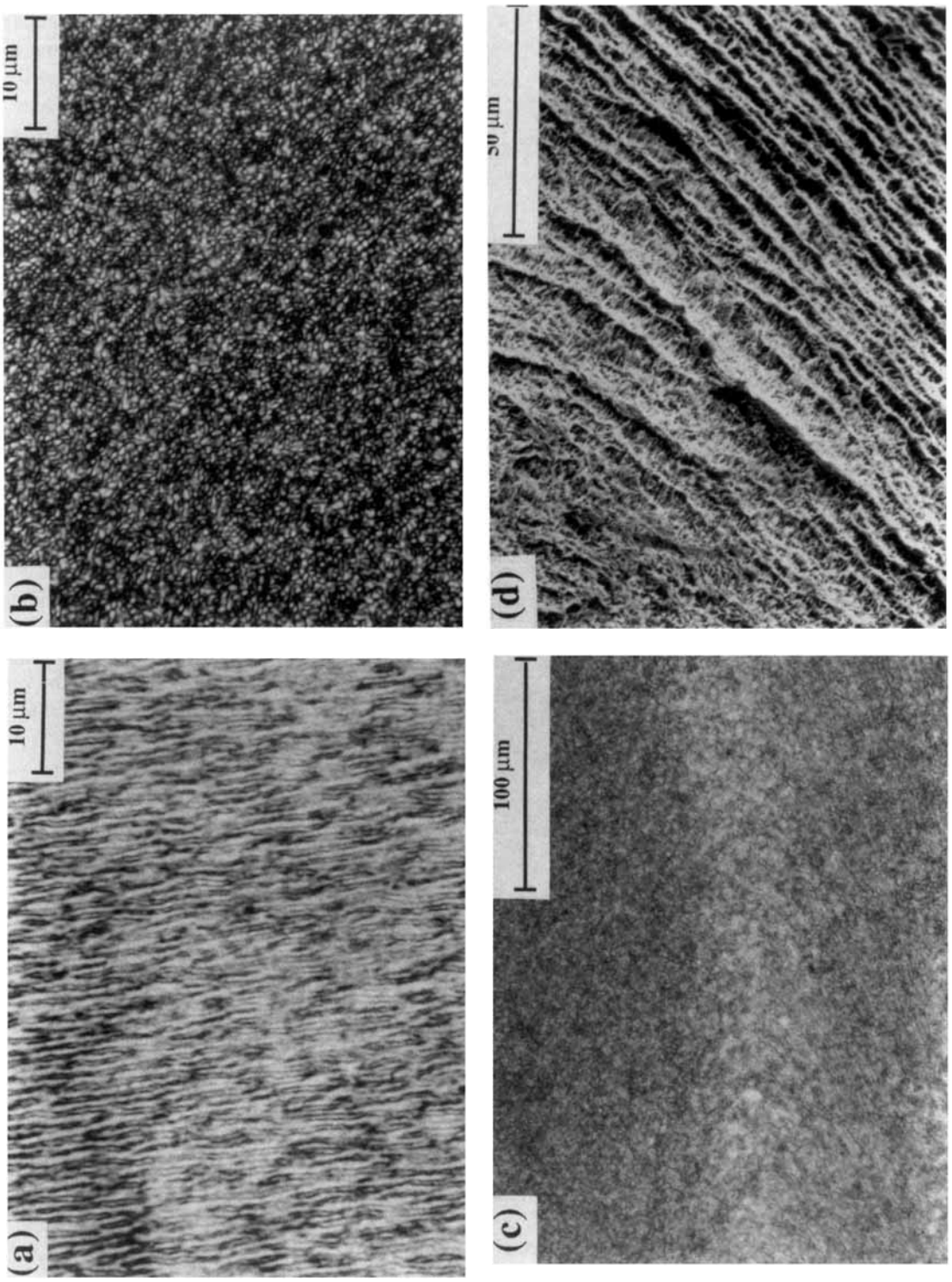

Figure 6 Optical investigation of longitudinal thin polished sections of unfilled HBA–HNA moldings (A950) under crossed polarizers: (a) inner skin; (b) intermediate layer; (c) inner core of 2 mm-thick plaque; (d) SEM of etched section corresponding to (iii).

there is often a high degree of transverse fiber orientation in the core (in the plane of the plaque).

3.3. Property Profiles within Samples

In what follows, results are given for the various measurement techniques described at the end of Section 2 for the 3 × 6 mm^2 Vectra moldings, characterization having been carried out as a preliminary to a series of bulk mechanical tests on these samples, to be described elsewhere.[41] For the purposes of comparison, the basic room temperature bulk tensile properties of the samples are summarized in Table I.

3.3.1. Modulus Profiles by Layer Removal

By measuring the modulus before and after removal of a thin layer from the sample, we have been able to construct modulus profiles as shown in Figure 9 for the 3 × 6 mm^2 cross-section filled and unfilled moldings. The stress–strain curve was recorded up to 0.01% extension (to avoid permanent deformation). A layer of chosen thickness was then cut from the sample surface using a rotary cutter and the stress–strain curve remeasured.

The method of analysis used in the literature[1] assumes a simple rule of mixtures, i.e., that a given layer contributes to the overall modulus in proportion to its thickness. One can then estimate the modulus of a given layer according to

$$E_l = \frac{E_s a_s - E_{s-1} a_{s-1}}{al} \qquad (1)$$

where E_l, E_s, and E_{s-1} are the moduli of the layer, the whole sample, and the sample without the layer, respectively, and a_l, a_s, and a_{s-1} are the corresponding cross sections.

Given that the error inherent in eq. (1) may exceed 30%, the E profiles obtained in this way are essentially qualitative, but reflect well the results of other workers.[1,16,31] In the unfilled samples, E is relatively large for a thin layer at the sample surface, but drops sharply further into the sample. At approximately 200 μm from the surface, there is a second large peak and, finally, a further, weaker peak at approximately 1 mm from the sample surface.

The positions of these peaks are found to correspond well to the outer and inner skins and to the intermediate layer–core boundary. According to Garg and Kenig,[1] the inner peaks arise from locally high shear rates where differing melt streams meet under nonisothermal conditions, from which one infers that the high orientation in the inner skin results from shear in regions adjacent to the solidified outer skin. This seems reasonable in view of the marked contrast in the textures of the outer and inner skin in etched cross sections and the fact that the banded optical texture observed in the inner skin appears typical of shear flow.

Somewhat surprisingly, in view of the microstructural changes described in Section 3.2, the 40 wt % wollastonite-filled moldings showed a similar modulus profile to that of the unfilled material, although the outer skin peak was either absent or not detectable by this method. There was also some suggestion of weak additional peaks in the inner regions of the filled samples.

3.3.2. Measurements on Removed Layers

This method can be used to measure the strength and extension to fail in different regions as well as the modulus. Its resolution is limited since handling and machining problems became critical for samples whose thickness was less than 300 μm. For the purpose of the present measurements, the samples were generally divided into the core, the intermediate region, and the skin, as identified by microscopical examination.

Typical results are illustrated for measurements on individual layers in Figure 10 for the 3 × 6 mm^2 samples. The skin regions in unfilled samples are characterized by high strengths and low extensions to fail relative to the intermediate layers. The extensions to fail of the skin regions are also similar to those of the whole moldings, suggesting that skin fracture determines the overall strength of these latter (as had previously been concluded for the 4 × 10 mm^2 samples[33]). The observation of low strains to fail in samples machined from the core of the unfilled 3 × 6 mm^2 samples is surprising in that there is no evidence for premature core failure during tests on the latter. In this case, the outer layers presumably concentrate strain energy away from defects in the core, such as the flow lines described in Section 3.1(iv).

For the particle-filled grades, addition of filler leads to a progressive decrease in the differences between the strengths of the different layers. Indeed, layers from 3 × 6 mm^2 moldings of the 40 wt % wollastonite-filled grade show little difference in tensile strength and similar high-strain behavior, as shown in Figure 10. The differences in strain to fail between the layers also appear less marked for 30 wt % glass fiber-filled samples than for the unfilled

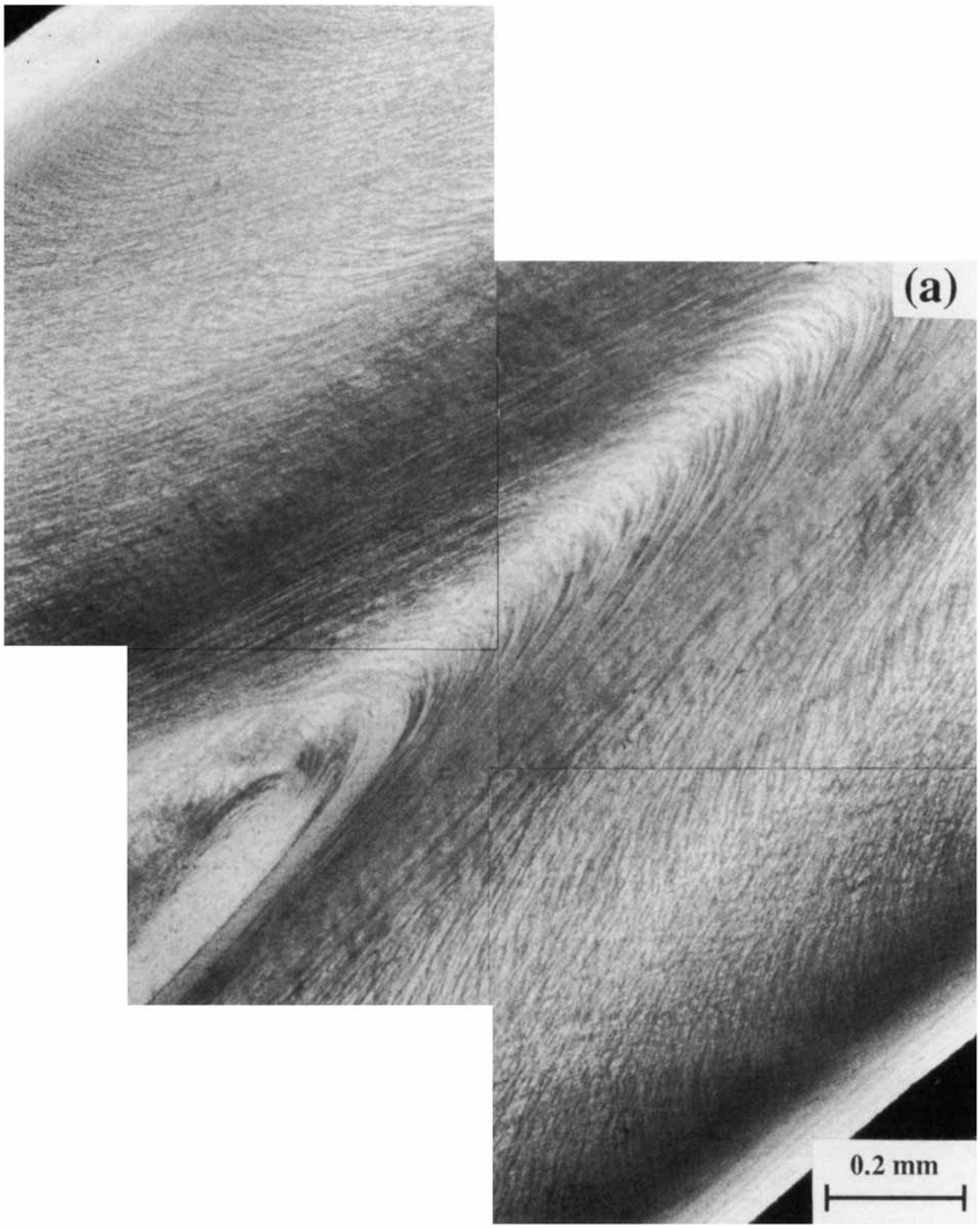

Figure 7 Core structures approximately midway along an Ultrax injection molding: (a) transmitted light micrograph under crossed-polarizers of a thin longitudinal section; (b) higher magnification of part of the core in the same molding; (c) SEM of a longitudinal fracture surface corresponding to (b).

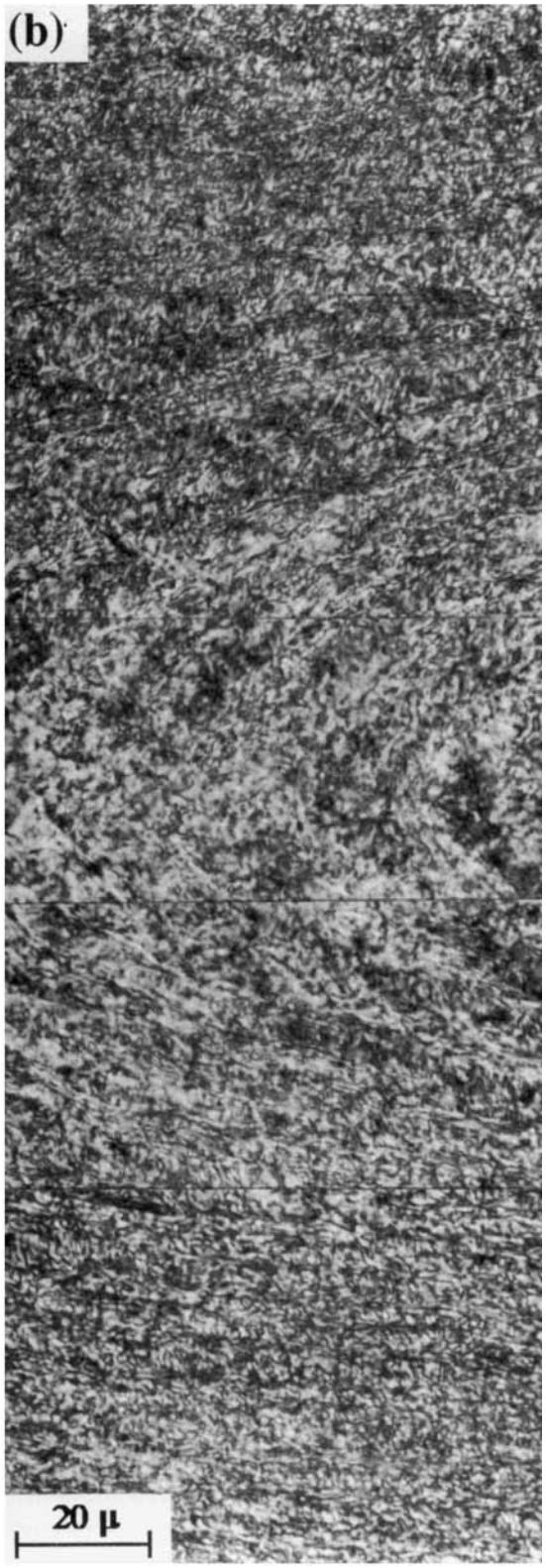

Figure 7 *(Continued from the Previous Page)*

samples, although there remains a significant difference in strength between the skin and core.

WAXS measurements were used to determine orientation of the layers, using the method detailed in Ref. 16. The orientation is characterized in terms of the Hermans orientation function, S, as defined by

$$S = \tfrac{1}{2}(3\langle \cos^2 \Theta \rangle - 1) \qquad (2)$$

where Θ is the angle between a given molecule and the main orientation direction, such that $S = 1$ for perfect alignment and $S = 0$ for random orientation. The results shown in Figure 11 are averaged over three separate measurements on samples of the order of a centimeter in length taken from either end of the sample barrel (i.e., adjacent to and opposite the gate). They are generally indicative of an increase in orientation in the outer layers of the samples as compared with the core and also a drop in orientation in the regions of the sample barrel furthest from the gate. In the unfilled sample, however, it is the intermediate layer rather than the surface layer that shows the highest mean orientation, in spite of the elevated tensile strength of skin indicated in Figure 10. Given the presence of large fluctuations in local orientation close to the surface implied by the modulus profiles in Figure 9, it is perhaps significant that the X-ray measurements were carried out on 300 μm-thick samples, whereas the skin layer in Figure 10 was 200 μm thick. Indeed, the tensile properties of 300 μm-thick layers taken from the surface of the unfilled samples were found to be similar to those of the intermediate layer (although with a reduced strain to fail of approximately 4%).

Figure 11 also suggests a tendency for wollastonite addition to even out the differences in orientation in the different layers, although the overall level of orientation does not appear to drop substantially in these samples. As shown in Figure 12, there is a clear correlation between the modulus of removed layers and S in the unfilled and filled samples (this in spite of the uncertainties regarding the homogeneity of the layers). Clearly, filler addition increases the modulus for a given value of orientation, and since the level of orientation is substantially retained, this translates into a progressive improvement in the bulk modulus of the samples with increasing filler content, as indicated in Table I.

There appears some evidence for a correlation between the tensile strength and the orientation in

Figure 7 (*Continued from the previous page*)

layer samples, with a decrease in strength with filler content for a given orientation.[33,34] However, since the strength will, in general, be reflected by the weakest link of an inhomogeneous structure, it is not clear that it should be directly linked to the orientation measurements of the type described here, whose resolution is considerably less than the spatial extent of features such as the flow lines described in Section 3.1. Moreover, the fact that filler addition decreases the strength suggests that the filler–matrix interface may itself represent a point of weakness, whose existence cannot be inferred from the measurement of matrix orientation. This may explain why the high-strain behavior and tensile strength appears less dependent on the orientation variations in the 40 wt % wollastonite-filled samples than on the (low-strain) Young's modulus. It should be emphasized, however, that this is merely a tendency. Forty percent wollastonite-filled samples remain highly anisotropic,[41] and somewhat larger differences in the longitudinal strengths of the skin and core have been seen in 40% wollastonite-filled 4×10 mm^2 cross-section samples, depending on the molding conditions.[34] They are certainly to be expected where there is a variation in orientation of high-aspect ratio fillers such as short glass fibers.

3.3.3. Modeling Using Aggregate Theory

The rigid rod nature of TLCP molecules makes TLCPs an ideal application for the Ward aggregate model.[42] The aggregate model averages the elastic constants of subunits, which may correspond either to individual molecules or subregions of perfect alignment, over a given or measured orientation distribution to give the macroscopic compliance/stiffness tensor. In general, it is found that better results are obtained if the average is performed assuming a constant stress condition (Reuss average). In this case, each of the expressions given by Ward[42]

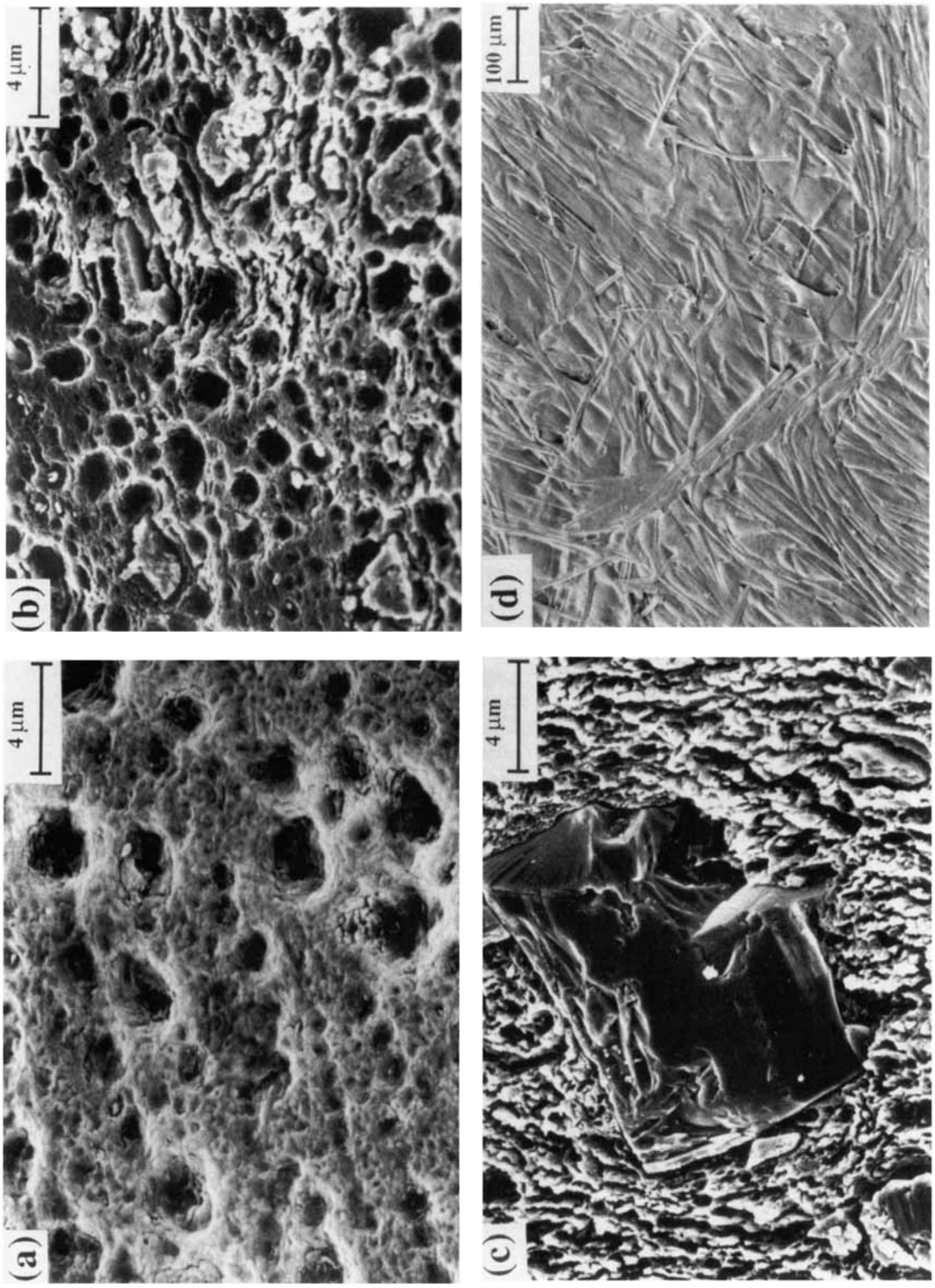

Figure 8 The effect of filler addition: (a–c) etched transverse sections from outer core region for HBA–HNA, HBA–HNA/15 wt % wollastonite, and HBA–HNA/40 wt % wollastonite, respectively; (d) surface (unetched) of HBA–HNA/30 wt % short glass fiber.

Table I Approximate Bulk Tensile Properties at Room Temperature for 3 × 6 mm² Cross-Section Vectra Moldings (Crosshead Speed 10 mm/min)

Filler	Strength (MPa)	Modulus (GPa)	Failure Strain (%)
Unfilled	190	11	4.2
30 wt % glass fiber	150	17	1.7
15 wt % wollastonite	170	14	4.0
40 wt % wollastonite	150	17	2.9

for the components of compliance tensor for the aggregate S_a takes the form

$$S_{i_a} = \sum A_{ij} S_j \qquad (3)$$

where S_j are the components of the compliance tensor for the subunits and A_{ij} are linear combinations of $\langle \cos^2 \Theta \rangle$ and $\langle \cos^4 \Theta \rangle$ corresponding to the orientation distribution of the subunits. The subunit compliances required for the model calculation are[16]

$$S_{33} = 1/E_3$$

$$S_{11} = 1/E_1$$

$$S_{13} = -\nu_{13} S_{33}$$

$$S_{12} = -\nu_{21} S_{11}$$

$$S_{44} = 1/G$$

where E_3, E_1, and G are, respectively, the axial, transverse, and shear moduli of the subunits.

It has been shown by Blundell et al. that by using values for the unit elastic constants estimated from highly oriented samples (E_3 = 100 GN m^{-2}; E_1 = 2 GN m^{-2}; G = 1 GN m^{-2}; $\nu_{13} = \nu_{21}$ = 0.4) and X-ray measurements of orientation distributions in injection moldings reasonable predictions for the Young's modulus may be obtained by using a combination of the Ward model for individual samples layers and simple laminate theory.[16] In Figure 13, the consequences of the model for the room-temperature modulus as a function of the orientation for unfilled Vectra are shown in comparison with our own X-

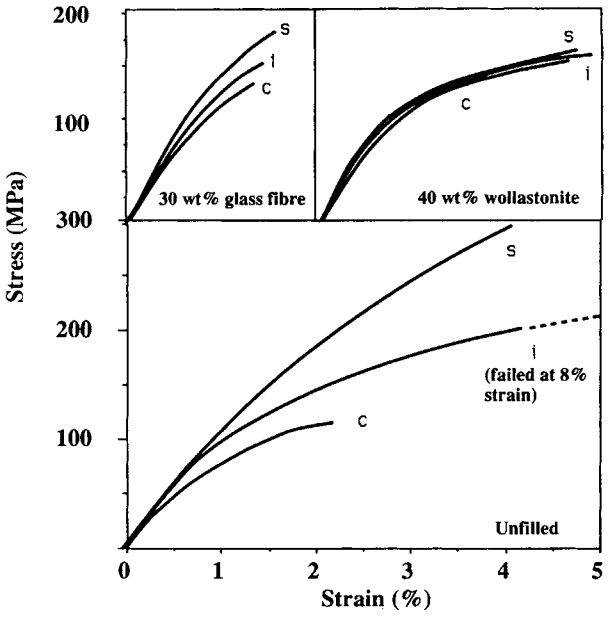

Figure 10 Stress–strain curves for individual layers in 3 × 6 mm² injection moldings (crosshead speed 10 mm/min): s, surface layer 6 × 0.2 mm²; i, intermediate layer, 5 × 0.4 mm² centered at 0.5 mm into the sample; c, 3 × 0.4 mm² from center of sample.

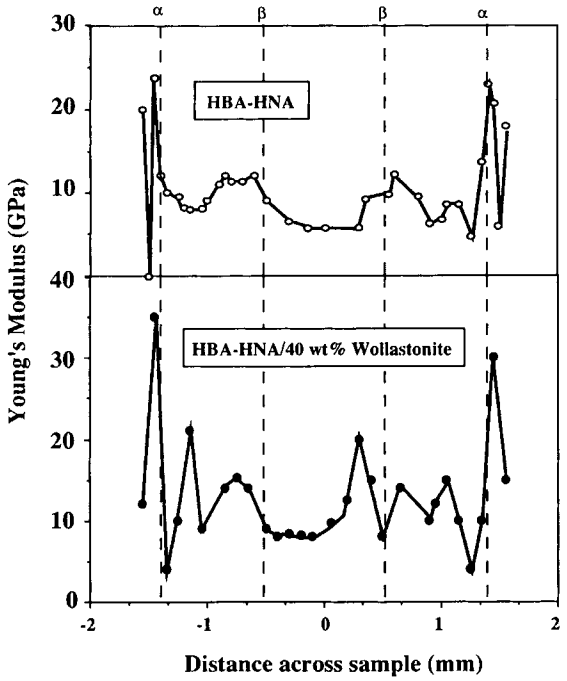

Figure 9 Modulus profiles for unfilled and filled 3 × 6 mm² cross-section injection moldings (crosshead speed 1 mm/min). α and β are the approximate positions of the skin–intermediate region and the intermediate region–core boundaries, respectively, as determined from morphological investigations.

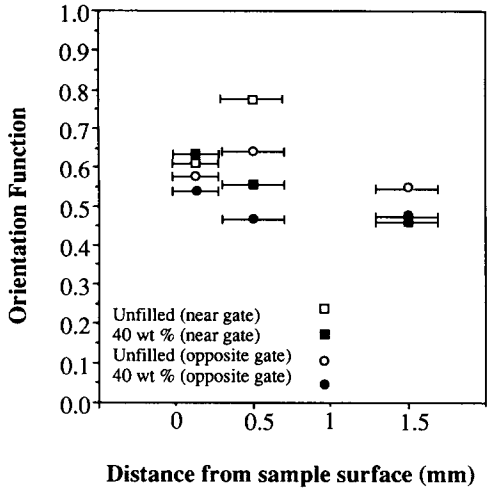

Figure 11 WAXS measurements of the extent of orientation in layers of the unfilled and 40 wt % wollastonite-filled 3 × 6 mm² injection moldings; error bars indicate the width of each layer.

ray data (replotted from Fig. 12). Also given for comparison are data for extruded TLCPS from Ref. 43. (The model prediction has been interpolated for S between 0.8 and 1, since values of $\langle \cos^4 \Theta \rangle$ were not given in Ref. 43.) Reasonable agreement is obtained, in spite of the possibility of through thickness orientation variations in the layer samples. Moreover, it is seen that the range of orientations typically encountered in our injection moldings is one in which the modulus changes relatively slowly with orientation. It is only for higher orientations such as those obtained by extrusion or fiber spinning that the modulus increases rapidly toward values close to E_{33}.

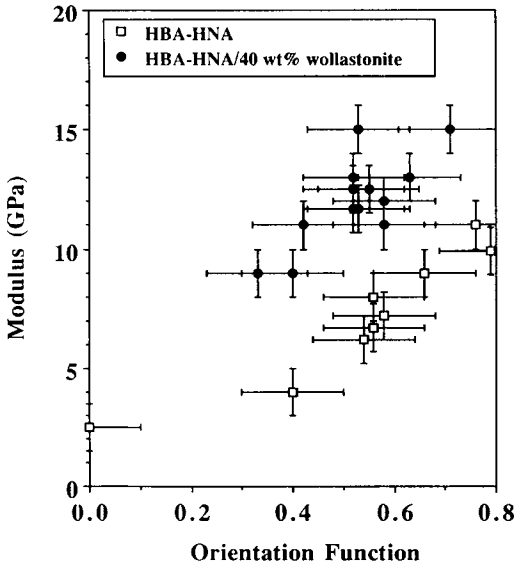

Figure 12 Modulus–orientation profiles for layers removed from filled and unfilled 3 × 6 mm² samples.

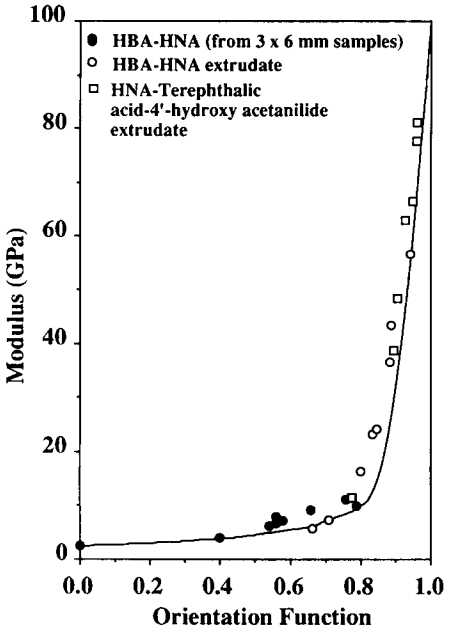

Figure 13 Comparison of aggregate model predictions for the modulus measured along the orientation direction ($1/S_{33a}$) and data from layers taken from 3 × 6 mm² injection moldings. Also given are data for extrudates taken from Ref. 43. The following values for the unit elastic constants were assumed, following Ref. 16: E_3 = 100 GN m^{-2}; E_1 = 2 GN m^{-2}; G = 1 GN m^{-2}; $\nu_{13} = \nu_{21}$ = 0.4.

4. CONCLUSIONS

We have presented the results of our own investigations of structure in in-house and as-received injection moldings of both Vectra and amorphous Ultrax. These show many similarities and are consistent with the overall picture presented in the literature. Using etching techniques, a loss of coarse structure in injection moldings containing mineral-filler particles has been demonstrated. However, this does not appear to be accompanied by a substantial loss in orientation at the molecular level in 3 × 6 mm² cross-section samples, so that the tensile modulus is improved on filler addition and there is only a moderate decrease in tensile strength.

Financial support from the Swiss Commission pour l'Encouragement de la Recherche Scientifique (CERS) is gratefully acknowledged. Special thanks are due to H.

Terwyen, Hoechst AG, Frankfurt am Main, and Professor W. Kaiser, HTL Brugg, for supplying some of the specimens.

REFERENCES

1. S. K. Garg and S. Kenig, in *High Modulus Polymers*, A. Z. Zachariades and R. S. Porter, Eds., Marcel Dekker, New York, 1988.
2. Z. Ophir and Y. Ide, *Polym. Eng. Sci.*, **23,** 792 (1983).
3. G. Menges, T. Schacht, H. Becker, and S. Ott, *Int. Polym. Process.*, **2,** 77 (1987).
4. H. Tharpar and M. Bevis, *J. Mat. Sci. Lett.*, **2,** 733 (1983).
5. L. C. Sawyer and M. Jaffe, *J. Mat. Sci.*, **21,** 1897 (1986).
6. E. G. Joseph, G. L. Wilkes, and D. G. Baird, *Polymer*, **26,** 689 (1985).
7. E. G. Joseph, G. L. Wilkes, and D. G. Baird, *Polym. Eng. Sci.*, **25,** 377 (1985).
8. G. G. Viola, D. G. Baird, and G. L. Wilkes, *Polym. Eng. Sci.*, **25,** 888 (1985).
9. T. Weng, A. Hiltner, and E. Baer, *J. Mat. Sci.*, **21,** 744 (1986).
11. S. Kenig, B. Trattner, and H. Andermann, *Polym. Compos.*, **9,** 20 (1988).
12. A. Pirnia and C. S. P. Sung, *Macromolecules*, **21,** 2699 (1988).
13. E. Suokas, J. Sarlin, and P. Törmälä, *Mol. Cryst. Liq. Cryst.*, **153,** 515 (1987).
14. A. Boldizar, *Plast. Rubber Process. Appl.*, **10,** 73 (1988).
15. E. Suokas, *Polymer*, **30,** 1105 (1989).
16. D. J. Blundell, R. A. Chivers, A. D. Curson, J. C. Love, and W. A. MacDonald, *Polymer*, **29,** 1459 (1988).
17. P. F. Bright, R. J. Crowson, and M. J. Folkes, *J. Mat. Sci.*, **13,** 2497 (1978).
18. M. J. Folkes, *Short Fibre Reinforced Thermoplastics*, Wiley, Chichester, U.K., 1982.
19. E. S. Clark., *Appl. Polym. Symp..*, **24,** 45 (1974).
20. J. Bowman, *J. Mat. Sci.*, **16,** 1151 (1981).
21. S. Kenig, *Polym. Compos.*, **7,** 50 (1986).
22. Y. Ide and Z. Ophir, *Polym. Eng. Sci.*, **23,** 261 (1983).
23. L. A. Goettler, *Polym. Compos.*, **5,** 60 (1984).
24. S. Onogi and T. Asada, Rheology, Vol. 1, G. Astarita, G. Marrucci, and L. Nicolais, Eds., Plenum Press, New York, 1980.
25. N. J. Alderman and M. R. Mackley, *Faraday Discuss. Chem. Soc.*, **79,** 149 (1985).
26. G. Marrucci and P. L. Maffettone, *Macromolecules*, **22,** 4076 (1989).
27. G. Marrucci and P. L. Maffettone, *J. Rheol.*, **34,** 1217, 1231 (1990).
28. M. Cenzig Altan, *J. Thermoplast. Compos.*, **3,** 275 (1990).
29. M. G. Dobb, D. J. Johnson, and B. P. Saville, *J. Poly. Sci. Poly. Symp.*, **58,** 237 (1977).
30. L. C. Sawyer, *J. Poly. Sci. Poly. Lett. Ed.*, **22,** 347 (1984).
31. W. J. Tomlinson and P. E. Morton, *J. Mat. Sci. Lett.*, **10,** 154 (1991).
32. M. Diez, C. Bader, and W. Kaiser, *Kunststoffe*, **81,** 705 (1991).
33. B. Zülle, A. Demarmels, C. J. G. Plummer, T. Schneider, and H.-H. Kausch, *J. Mat. Sci. Lett.*, to appear.
34. B. Zülle, A. Demarmels, C. J. G. Plummer, and H.-H. Kausch, to appear.
35. C. Viney, A. M. Donald, and A. H. Windle, *J. Mat. Sci.*, **18,** 1136 (1983).
36. D. J. Graziano and M. R. Mackley, *Mol. Cryst. Liq. Cryst.*, **108,** 73 (1984).
37. A. M. Donald and A. H. Windle, *J. Mat. Sci.*, **19,** 2085 (1984).
38. A. M. Donald and A. H. Windle, in *Recent Advances in Liquid Crystalline Polymers*, L. L. Chapoy, Ed., Elsevier, New York, 1985. P. Navard, *J. Polym. Sci. Polym. Phys. Ed.*, **24,** 435 (1986).
39. C. Viney, A. M. Donald, and A. H. Windle, *Polymer*, **26,** 870 (1985).
40. D. T. Stell, A. M. Donald, and W. A. MacDonald, in *Proceedings of the Sixth Annual Meeting, Polymer Processing Society*, Nice, April, 1990.
41. C. J. G. Plummer, P. Davies, H.-H. Kausch, B. Zülle, and A. Demarmels, to appear.
42. I. Ward, *Proc. Phys. R. Soc.*, **80,** 1176 (1962).
43. T.-S. Chung, *J. Polym. Sci. Polym. Lett.*, **24,** 299 (1986).

Received May 28, 1992
Accepted July 28, 1992